Efficiency of TiO2 photocatalytic degradation of HHCB(1,3,4,6,7,8-hexahydro-4,6,6,7,8,8-hexamethylcyclopenta[]-2-benzopyran) innatural aqueous solutions by nested experimental design and mechanism ofdegradation

Efficiency of TiO_2 photocatalytic degradation of HHCB (1,3,4,6,7,8-hexahydro-4,6,6,7,8,8-hexamethylcyclopenta[γ]-2-benzopyran) in natural aqueous solutions by Nested Experimental Design and mechanism of degradation

P. Calza[1], V.A. Sakkas[2], C. Medana[1], M. Azharul Islam[b], E. Raso[1], K. Panagiotou[b], T. Albanis[b]*

[1] Department of Analytical Chemistry, University of Torino, via P. Giuria 5, 10125 Torino, Italy

[2] Department of Chemistry, University of Ioannina, Ioannina 45110, Greece

**Corresponding author: Dr. V.A. Sakkas, Tel: +3026510-08303, Fax: +3026510-08795*

E-mail address: vsakkas@cc.uoi.gr

Abstract

The present paper deals with the photocatalytic transformation of HHCB (1,3,4,6,7,8-hexahydro-4,6,6,7,8,8-hexamethylcyclopenta[γ]-2-benzopyran, trade name Galaxolide), under simulated solar irradiation using titanium dioxide as a photocatalyst. The investigation has involved a study of HHCB decomposition under a variety of experimental conditions, the identification of intermediate compounds, as well as the assessment of mineralization. A fully nested experimental design was applied to study the effect of various matrices (i.e. distilled water, surface water and wastewater) as well as the initial HHCB concentration on the variation of the photocatalytic efficiency. GC/MS and LC/MS were brought to bear in assessing the temporal course of the photocatalyzed process. A first pathway involves the hydroxylation, that is confined to the benzopyran moiety. Another route proceeds through the detachment of the hexamethylpentacycle moiety, with the formation of the ketoderivative. A parallel transformation involves benzopyran moiety with the ring cleavage. All the identified transformation products are degraded themselves until 2 h of irradiation, while complete mineralization is achieved until 8h.

1. Introduction

Synthetic musk fragrances are essential ingredients widely used in numerous perfumes, cosmetics and cosmetic care products, soaps, detergents, and other cleaning agents [1] and [2]. Production and usage of nitro musks (such as musk xylene and musk ketone) have decreased since the late 1980s, due to concerns about toxicity [3]. Conversely, the use of the two most important compounds of polycyclic musks, hexahydro-4,6,6,7,8,8-hexamethylcyclopenta(g)-2-benzopyran (HHCB) and 7-acetyl-1,1,3,4,4,6-hexamethyltetrahydronaphthalene (AHTN) (representing about 95% of the total market volume for the class of fragrance ingredients) has increased in the last decade [3]. There is a great potential for these chemicals to go down the drain, subsequently reaching wastewater treatment plants (WWTPs). Thus, release through WWTPs is a pathway for the contamination of aquatic environment such as rivers, lakes, and estuaries and exposure of aquatic biota. This, combined with high log Kow values and lack of ready biodegradability, has resulted in their widespread occurrence in the environment [4]. Several studies have reported the occurrence of synthetic musks such as HHCB in WWTPs, surface waters, biota, including fish and marine mammals as well as air [3,5-7].

Because surface water is the most affected, personal care products (PPCPs) may first pose a problem to utilities that use surface water as a source for drinking water production. Therefore, a crucial need for more enhanced technologies that can reduce their presence in the environment has become evident. In the last few years, new technologies for the decomposition of organic micro-pollutants in the aqueous environment have been developed. Heterogeneous photocatalysis [8] and [9] represents an example of advanced oxidation processes (AOPs) capable of achieving a complete oxidation of large variety of organic and inorganic species, including dyes, pesticides, endocrine disrupting chemicals (EDCs), pharmaceuticals, PPCPs etc. [10-16].

The use of chemometric methods based on statistical design of experiments (DOEs) is becoming increasingly widespread in several sciences such as analytical chemistry, engineering and environmental chemistry. Applied catalysis, is certainly not the exception. It is clear that photocatalytic processes mated with chemometric experimental design play a crucial role in the ability of understanding the statistically significant variables affecting the process and reaching the optimum of the catalytic reactions.

In the present challenging work, TiO_2 photocatalytic oxidation of HHCB was investigated with the scope of determining the degree of reproducibility of the oxidation process under a variety of conditions such as initial substrate concentration, and water matrix, by the employment of chemometrics. For this reason a fully nested experimental design approach was employed to determine the variation of the process with regards to HHCB photocatalytic yield. In analogy with the effects calculated from screening designs these variations give information about the influence of a factor on a response. This information is very essential for photocatalytic studies since from a practical point of view there is a need to investigate the application of TiO_2 for the degradation of the target contaminants at environmental concentrations and at real surface water or wastewaters. Since these matrices are complex, the AOPs have to be carefully operated in order to avoid incomplete mineralization of organic contaminants which may result in the formation of oxidation intermediates which can be more dangerous than the parent compounds.

Another aspect of this work was the identification of possible intermediate products. For this reason powerful analytical techniques such as liquid chromatography coupled to mass spectrometry was employed. To the best of our knowledge this is the first time that an extensive study of the photocatalyzed transformation of the polycyclic musk HHCB is studied.

2. Experimental

2.1. Material and reagents

1,3,4,6,7,8-hexahydro-4,6,6,7,8,8-hexamethylcyclopenta[γ]-2-benzopyran, (HHCB) with purity higher than 99% was supplied by LGC Promochem Iberia (Wesel, Germany). All solvents used were obtained from Merck (Darmstadt, Germany). HPLC grade methanol (BDH) was filtered through a 0.45 μm filter before use.

Experiments were carried out using TiO_2 Degussa P25 as the photocatalyst. In order to avoid possible interference from ions adsorbed on the photocatalyst, the TiO_2 powder was irradiated and washed with distilled water.

2.2. Irradiation procedures

Irradiation experiments of HHCB in two natural waters, as well as in distilled water, were carried out on stirred aqueous solutions contained in a cylindrical quartz glass UV reactor (maximum capacity 75 mL). Degradations were performed on 50 mL of aqueous HHCB solutions with varying initial concentrations 1, 50 and 100 μg/L at a fixed concentration of TiO_2 (200 mg/L), according to the experimental design (Table 1). Before irradiation, the suspensions were allowed to stay in the dark for 60 min under stirring, to reach adsorption equilibrium on the semiconductor surface. Irradiation was carried out using a Suntest CPS+ apparatus from Heraeus (Hanau, Germany) equipped with a xenon arc lamp (1500W) and special glass filters restricting the transmission of wavelengths below 290 nm. Chamber and black panel temperature were regulated by pressurized

air cooling circuit and monitored using thermocouples supplied by the manufacturer. The light source was on the top of the reactor and an average irradiation intensity of 750 W m^{-2} was maintained throughout the experiments. The temperature of samples did not exceed 20^{o} C using tap water cooling circuit for the UV-reactor. To remove TiO_2 particles the solution samples were passed through 0.45 mm HA cellulose acetate membrane filters and were further analyzed by the appropriate analytical technique.

The degradation efficiency (expressed as % degradation) was calculated as:

% degradation = $100 \times \frac{C_o - C_f}{C_o}$, where *C*o the initial concentrations of HHCB and C_f the final concentrations of HHCB in the solutions, after 20 min of irradiation in the presence of titania.

Experiments on intermediates have been performed in air saturated conditions using a Philips TLK/05 lamp (40 W/m^2) with the maximum emission at 360 nm. Irradiation experiments were carried out in pyrex glass cells containing 5 ml of HHCB (15 mg/L) and TiO_2 (200 mg/L) in distilled water. The temperature reached during the irradiation was 38 ± 2°C. The entire content of the cells was filtered through a 0.45 μm filter and then analyzed with the appropriate techniques.

2.3. Analytical procedures

2.3.1. Analytical techniques and gas chromatography

In the experiments where kinetics studies have been performed, during illumination of the aqueous solution, samples were withdrawn from the reactor at specific time intervals. The aqueous samples were filtered through 0.45 mm Millipore disks to remove TiO_2 particles and were extracted with a recently developed microextraction method, dispersive liquid-liquid microextraction (DLLME) [17]. Five milliliters (5.00 mL) of aqueous sample was placed in a 10 mL screw cap glass test tube

with conical bottom. 0.62 mL of methanol (as disperser solvent) containing 250 μL CCl_4 (as extraction solvent) were rapidly injected into the sample solution with a 5.00 mL glass syringe and the mixture was gently shaken. In this step, a cloudy solution was formed and the analytes in the water sample were extracted into fine droplets. The mixture was then centrifuged for 7.5 min at 4000 rpm. After centrifuging the volume of the sedimented phase (CCl_4) was concentrated to 20 μL under a gentle steam of nitrogen and was determined at GC–MS.

A Shimadzu GC 17A gas chromatograph, coupled to a QP-5000 mass spectrometer was used for the determination of the degradation efficiency of HHCB. Chromatographic separation was accomplished with a DB-5MS (J & W, Folsom, CA, USA) fused-silica capillary column (30 m, 0.32 mm, I.D. 0.25mm) coated with a 5% biphenyl–95% dimethylsiloxane stationary phase. Helium was the carrier gas at a flow-rate of 1.2 mL/min. The GC oven temperature program was as follows: initial temperature 50 ◦C for 2min, 20° C/min to 190 ◦C, 5° C/min to 270 ◦C and held for 5 min. The temperatures of the ion source and the interface were set at 280 ◦C. The mass spectrometer was operated in the electron impact (70 eV), selected ion monitoring (SIM) mode at 1.50 kV. Ions at *m/z* = 243, 258, and 213 were used for identification and quantification purposes, respectively.

For byproduct analysis, solid-phase microextraction with subsequent GC/MS analysis has been employed for identification of intermediates. The SPME manual holder and fibres were obtained from Supelco (Bellefonte, PA, USA). In this work, 100 mm fibres coated with polydimethylsiloxane (PDMS) were used. The fibres were conditioned following the manufacturer's recommendations. The sample was kept under magnetic stirring at 40 °C and the fiber was exposed for 20 min.

Analyses were run on a gas chromatograph (Agilent 6890, series II) equipped with a 5% phenylmethylpolysiloxane column (Agilent HP-5; 30 m × 0.25 mm). The GC operating parameters were as follows: injector at 300°C, splitless injection (1 min), volume injected 1 μL. The analysis

were performed using a double gradient. Temperature was linearly increased at 10 °C/min from 50 to 250 °C and then was brought to 300 °C at a rate of 20°C/min. The mass spectrometer was operated scan mode in the mass range 40-500.

2.3.3. Liquid chromatography-mass spectrometry

The chromatographic separations followed by a MS analyzer were run on a C18 column Phenomenex Sinergi, 150 × 2.0 mm using an Ultimate 3000 HPLC instrument (Dionex). Injection volume was 20 μL and flow rate 200 μL/min. Gradient mobile phase composition was adopted: 5/95 to 100/0 in 21 min. acetonitrile/formic acid 0.05% in water, then 5 min. 100/0, 1 min. 100/0 to 5/95 and other 5 min. 5/95.

A LTQ Orbitrap mass spectrometer (ThermoFisher) equipped with an atmospheric pressure interface and an ESI ion source was used as detector. The LC column effluent was delivered into the ion source using nitrogen as sheath and auxiliary gas. The source voltage was set at the 4.5 kV value. The heated capillary value was maintained at 265°C. The acquisition method used was previously optimized in the tuning sections for the parent compound (capillary, magnetic lenses and collimating octapoles voltages) in order to achieve the maximum of sensitivity. The tuning parameters adopted for ESI source have been the following: positive ion mode: capillary voltage 11.02 V, tube lens 65 V; for ions optics, multipole 00 offset -2.00 V, lens 0 voltage -4.00 V, multipole 0 offset - 4.50 V, lens 1 voltage -10.00 V, gate lens voltage -74.00 V, multipole 1 offset -11.00 V, front lens voltage -4.75 V; negative ion mode: capillary voltage -7.0 V, tube lens -44 V; for ions optics, multipole 00 offset 2.50 V, lens 0 voltage 2.00 V, multipole 0 offset 6.00 V, lens 1 voltage 9.00 V, gate lens voltage 54.00 V, multipole 1 offset 6.00 V, front lens voltage 6.00 V. Mass accuracy of recorded ions (vs calculated) was ± 15 millimass units (mmu) (without internal calibration).

2.3.4. Total organic carbon analyzer

Total organic carbon (TOC) was measured on filtered suspensions using a Shimadzu TOC-5000 analyzer (catalytic oxidation on Pt at 680 °C). The calibration was performed using standards of potassium phthalate.

2.3.6. Experimental design

In order to calculate the variation of the photocatalytic efficiency (expressed as % degradation), a fully nested experiment of three factors, that is, matrices (distilled water, lake water and wastewater), HHCB initial concentration (1, 50 and 100 μg/L) as well as replicates, was conducted. The design is called nested because the subordinate classification is nested within the higher classification level. The experimental set-up is shown in Fig.1. Matrix was placed in the highest rank of hierarchy being followed by initial HHCB concentration and replicates, (considering the requirement that factor most affected by systematic effects should be arranged in the highest ranks of the hierarchy and those affected mainly by random effects should be in the lowest ranks of the design). The lowest factor is considered to have a residual variation. The photocatalytic efficiency (response) was calculated for three aqueous matrices of different nature (distilled, lake and wastewater, l = 3). For each matrix, the percentage of photocatalytic degradation was calculated on three concentration levels (p = 3), that is, 1, 50 and 100 μg/L. Finally three replications of each concentration level are considered in the experiment (r = 3). The applied fully nested design was consisted of 27 experiments; the detail design matrix is presented in Table 1.

Design-Expert software (trail version 7, Stat-Ease, Inc., MN) was used for the data analysis according to the proposed method by Montgomery (2008) [18].

3. Results and discussion

Preliminary experiments were carried out, before the development of the experimental design, to evaluate the extent of hydrolysis and photolysis processes on the HHCB transformation. Results obtained from the adsorption in the dark, hydrolysis as well as direct photolysis for a time period of 90 min showed that the above abiotic processes were scarcely responsible for the observed fast transformations when the solution was irradiated in the presence of the TiO_2.

3.1. Assessment of variation

The objective of the present nested experiment was to explore the source of variation for the photocatalytic degradation of HHCB under different conditions. For this reason, a stepwise separate ANOVA was performed in order to assess the variation of the catalytic process for each factor (matrix, substrate concentration, triplicates). These interpretations are based on F-tests, estimation of the variance and expressing these variances relative to the sum of all variances [19]. First we consider the variance estimated for each factor as the most interesting. These effects are calculated in such a way that when the effect of a factor is calculated, the influence of all other factors is canceled.

It can be seen from the ANOVA considering only the aqueous matrix (Table 2), that different types of water (distilled, lake and wastewater) are not statistically significant (p-value for probability> F is greater than 0.10) for the process. In other words results indicated that if we consider only the different water matrices, these did not cause large variation in the measured photocatalytic efficiency of HHCB. On the other hand, ANOVA for nested factors, indicated that initial HHCB

concentration has significant effect on the photocatalytic efficiency, while analysis of triplicates showed that this factor had a non significant effect causing negligible variation in the response.

Finally full model (all effects) considering sources of water, concentration and their interaction was fitted in order to get actual diagnostics and graphs (Fig. 2). As we can observe from the residual plot, the data were normally distributed indicating a good fit for the model. Besides, when the two mentioned factors (water matrix and HHCB initial concentration) were considered together and analyzed, then, significant effects with regards to the photocatalytic efficiency was obtained of all model parameters (ANOVA for all effects, Table 2).

From Fig. 3 we may observe that the photocatalytic degradation efficiency (% degradation) varied significantly within each water matrix from low to high concentration levels. In general for low initial HHCB concentration levels (1 μg/L), the degradation percentage was the highest and almost similar for all aqueous matrices. As the initial concentration of HHCB increases (50 μg/L) a variation of the degradation yield is observed depending on the water type and especially for wastewater. The observation is more pronounced at the highest HHCB concentration (100 μg/L) at which the photocatalytic degradation of wastewater is remarkably reduced compared to others. As clearly seen, the extent of degradation decreases in the order distilled water > lake water > wastewater and this may be attributed to (i) the increased organic carbon content in lake and wastewater samples (they contain about 10 and 20 mg/L DOC, respectively) which is expected to decrease HHCB conversion and (ii) the presence of various species (e.g. Cl^{-}, HCO_3^{-}, CO_3^{2-}) and other reactive moieties competing for $OH^{\cdot}$ radicals (scavengers) and photocatalyst surface sites.

On the other hand it is clear that the degradation efficiency decreases with an increase in concentration of HHCB from 1 to 100 μg/L, showing that the degradation rate can be described by pseudo first-order kinetics with respect to the concentration within the experimental range. While there is still an ongoing debate whether photocatalytic oxidation reactions are surface or solution

processes, in most cases data processing is performed employing the empirical Langmuir–Hinshelwood kinetic model. Increased concentration of the pollutant could occupy more active sites of TiO_2, which inhibits generation of the oxidants, reducing the efficiency of the catalytic reaction [20]. Another possible reason is the intermediate products formed upon photocatalytic degradation of HHCB may compete with the HHCB molecules for the limited adsorption and catalytic sites on the surface of catalyst particles, and thus inhibit the degradation of HHCB to a certain extent.

3.2. Transformation products

The study of the HHCB transformation process was performed in the presence of 200 mg/L TiO_2 in distilled water. Along with HHCB decomposition (see Fig. 4), the formation of several intermediate compounds occurred. HHCB disappearance and formation of hydrophobic compounds was followed by SPME/GC/MS, while more hydrophilic compounds were detected by HPLC/MS; their time evolution curves are shown in Fig. 5 and Fig. 6, respectively. The formed transformation products were easily degraded, as assessed by Fig. 5 and Fig. 6, and after 2 h of irradiation they were completely degraded. At that time, almost 50% of the organic carbon was mineralized (see Fig. 4); even if HHCB completely disappears within 15 min of irradiation, the total mineralization for organic carbon was only achieved after 8 h of irradiation.

HHCB initial transformation proceeded through the formation of six main intermediate compounds, whose *m/z* ratios, product ions and retention times are summarized in Tables 3 and 4. Three initial transformation products were only identified by HPLC/MS and other three transformation products were only detected by GC/MS.

Looking closer to the transformation products identified by GC/MS, their recognition was done by using an identification program by NIST library and the proposed structures are collected in

Table 3. Two transformation products were formed through the HHCB hydroxylation or the cleavage of the benzopyran moiety with the formation of 1,3,4,6,7,8-hexahydro-4,6,6,7,8,8-pentamethyl-oxo-cyclopenta[γ]-phenol. A third species was recognized as 1,3,4,6,7,8-hexahydro-4,6,6,7,8,8-pentamethyl-oxo-cyclopenta[γ]-dihydroxybenzene.

Table 4 shows the species detected by HPLC/HRMS. Analyses were run in positive and negative mode. ESI (+) appears to be more sensitive and suitable for most of the transformation products. The positive-ion ESI mass spectra of HHCB transformation products provided a simple means for the determination of the molecular mass. The proposed structures are consistent with the fragmentation profiles of their protonated forms, as will be described in details below.

Two isobaric species at $[M+H]^+$ 193.0464 are formed. High resolving power was useful for assigning to them an empirical formula, $C_{10}H_9O_4$, while their MS^2 and MS^3 spectra showed several structural-diagnostic ions that allowed for distinguishing the two isomers. The species labelled A eliminates an ethene molecule. In MS^3 fragmentation of $[MH-C_2H_4]^+$ two ions are generated: the first one (137.0210 *m/z*) is originated from the elimination of carbon monoxide; the second one (121.0263 *m/z*) from the CO_2 elimination, well matched with the structure proposed in Scheme 1A.

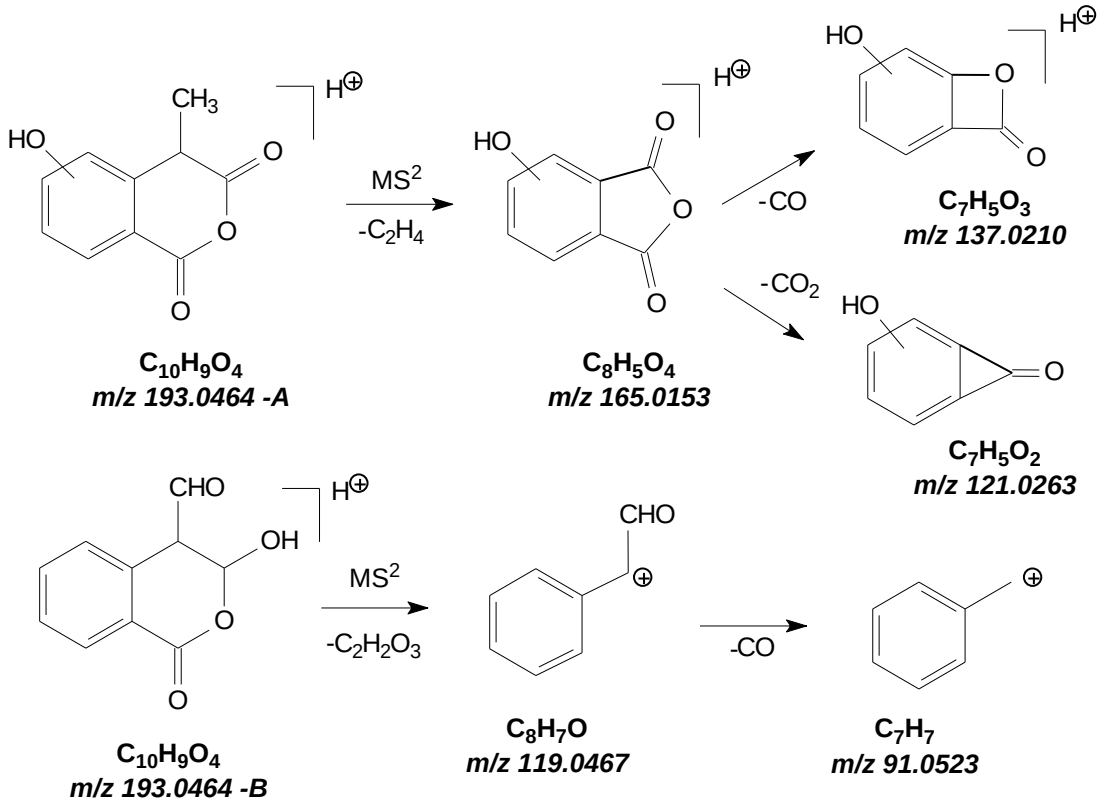

Scheme 1. Key fragmentation pathways followed by the species at m/z 193.0464

Conversely, the species labelled B loses a diformylether molecule with the formation of a product ion at *m/z* 119.0467, allowing for the proposition the structure shown in Scheme 1B. In MS^3 fragmentation of $[MH - C_2H_2O_3]^+$, CO is lost.

A third species at $[M+H]^+$ 235 was also detected; MS^2 key fragmentation allowed for assigning the structure shown is Scheme 2.

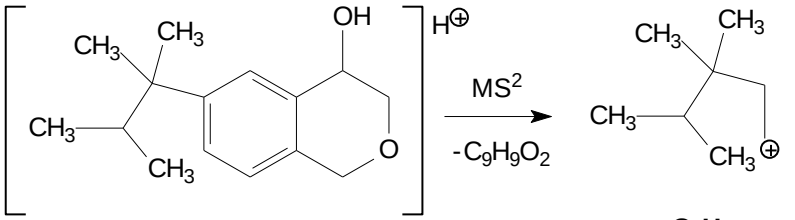

$C_{15}H_{23}O_2$
m/z 235.1809

C_8H_{17}
m/z 113.1303

Scheme 2. Key fragmentation pathways followed by the species at *m/z* 235.1809

HHCB lactone has been reported in some studies as a degradation product of HHCB [21]. In our experimental conditions, the presence of HHCB was found both at blank samples (without irradiation) as well as at irradiated samples. Therefore authors could not consider HHCB lactone as a proper HHCB photocatalytic transformation product.

Conclusions

The degradation of HHCB was studied by means of TiO_2 photocatalysis under simulated solar irradiation. The study included the investigation of the effect of various parameters such as initial substrate concentration, and water matrix. For this reason a fully nested experimental design approach was employed to determine the variation of the process with regards to HHCB photocatalytic yield. Results have shown that catalytic efficiency depends on both the aqueous

matrix and the initial concentration of the pollutant involved. The results clearly delineate the important role of the selection of the most appropriate reaction conditions in achieving highest removal efficiency for specific treatment cases.

HHCB was transformed under photocatalytic treatment into several species. The degradation compounds were identified by SPME/GC/MS and LC/HRMS. The benzopyran moiety was involved in hydroxylation and the ring cleavage, while another route proceeds through the detachment of the hexamethylpentacycle moiety, with the formation of the ketoderivative. The identified compounds are easily degraded within 2 h of irradiation and complete mineralization is accomplished within 8 h.

References:

[1] S. Schwartz, V. Berding, M. Matthies, Chemosphere 41 (2000) 671-679

[2] J. Reiner and K. Kannan, Chemosphere 62 (2006) 867–873

[3] Y. Horii, J. L. Reiner, B. G. Loganathan, K. Senthil Kumar, K. Sajwan, K. Kannan, Chemosphere 68 (2007) 2011–2020

[4] F. Balk, R. A. Ford, Tox Lett 111 (1999) 81–94

[5] H. Nakata, H. Sasaki, A. Takemura, M. Yoshioka, S. Tanabe, K. Kannan, , Environ. Sci. Technol. 41 (2007) 2216-2222

[6] K. Kannan, J.L Reiner, S.H. Yun, E.E Perrotta, L.Tao, B. Johnson-Restrepo, B.D. Rodan, Chemosphere 61 (2005) 693–700

[7] I.J. Buerge, H.-R. Buser, M.D. Muller, T. Poiger, Environ. Sci. Technol. 37 (2003) 5636–5644.

[8] P. Schneider, A. Bringhen, H. Gonzenbach, Drug Cosmet. Ind. 159 (1996) 32–38

[9] A. Fujishima, K. Hashimoto, T. Watanabe, TiO_2 Photocatalysis: Fundamentals and Applications, BKC Inc., Tokyo, 1999.

[10] P. Calza, V.A. Sakkas, C. Medana, C. Baiocchi, A. Dimou, E. Pelizzetti, T. Albanis, Appl. Catal. B: Environ. 67 (2006) 197–205

[11] P. Calza, V.A. Sakkas, A. Villioti, C. Massolino, V. Boti, E. Pelizzetti, T. Albanis, Appl. Catal. B: Environ. 84 (2008) 379–388

[12] S. Esplugas, D.M. Bila, L.G.T. Krause, M. Dezotti, J. Hazard. Mater. 149 (2007) 631–642

[13] J.M. Herrmann, J. Disdier, P. Pichat, S. Malato, J. Blanco, Appl. Catal. B: Environ. 17 (1998) 15–23

[14] V.A. Sakkas, P. Calza, C. Medana, A.E. Villioti, C. Baiocchi, E. Pelizzetti, T. Albanis, Appl. Catal. B: Environ. 77 (2007) 135–144.

[15] V.A. Sakkas, Md. Azharul Islam, C. Stalikas, T. A. Albanis, J Haz Mat 175, (2010) 33-44

[16] E. Hapeshi, A. Achilleos, M.I. Vasquez, C. Michael, N.P. Xekoukoulotakis, D. Mantzavinos, D. Kassinos, Wat Research 44 (2010) 1737–1746

[17] A. N. Panagiotou, V. A. Sakkas, T. A. Albanis, Anal Chim Acta 649 (2009) 135–140

[18] Montgomery, D.C. 2008. Design and Analysis of Experiments, 7th Edition, John Wiley & Sons Inc.

[19] Y. Vander Heyden, K. De Braekeleer, Y. Zhu, E. Roets, J. Hoogmartens, J. De Beer, D.L. Massart, J Pharmaceut Biomed Anal 20 (1999) 875–887

[20] Yang, L., Yu, L.E., Ray, M.B., Water Research 42 (2008) 3480–3488

[21] J.L. Reiner, J.D. Berset, K. Kannan, Arch. Contam. Toxicol. 52 (2007) 451-457

Legend for figures

Fig.1. Nested factorial design for photocatalytic degradation

Fig.2. Residual plots for fitted model

Fig.3. Scatter plot of actual photocatalytic degradation results

Fig.4. Degradation of HHCB 15 mg/L on TiO_2 200 mg/L; disappearance of the initial compound and TOC profile.

Fig.5. Intermediates formed from HHCB degradation as a function of the irradiation time and detected by GC/MS.

Fig.6. Intermediates formed from HHCB degradation as a function of the irradiation time and detected by HPLC/MS.

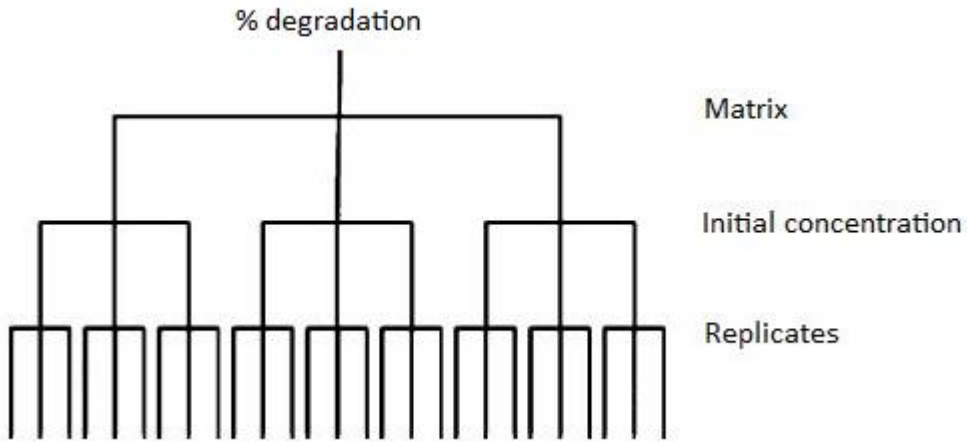

Fig.1

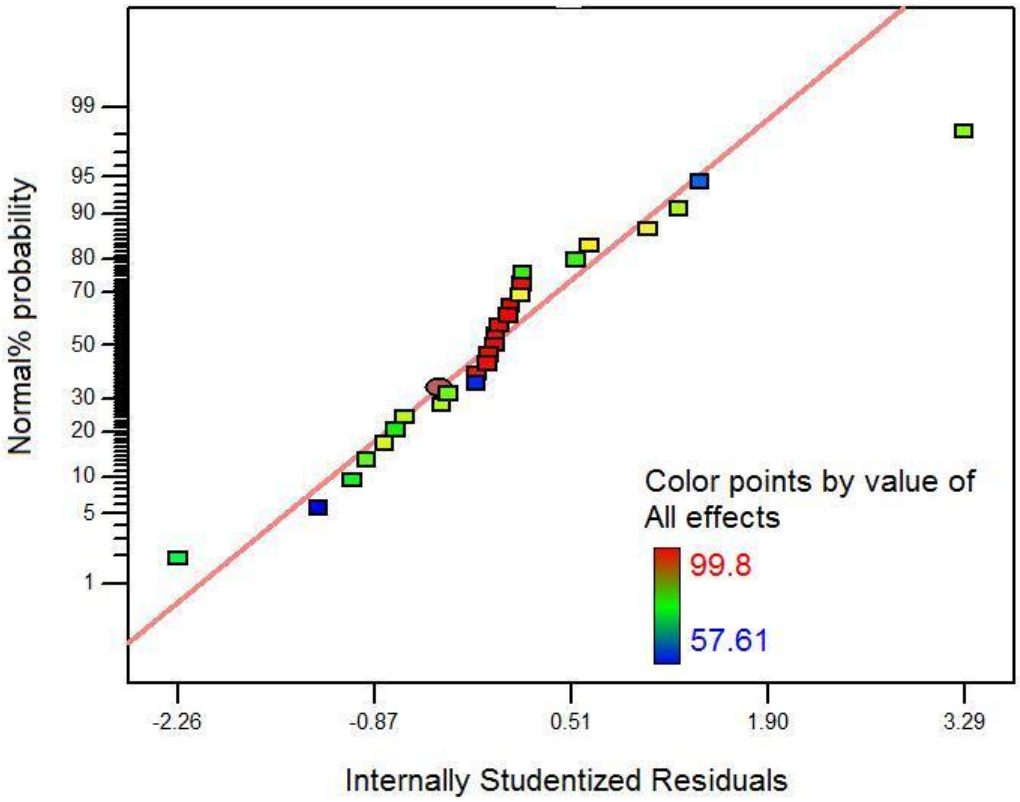
Normal% probability
99
95
90
80
70
50
30
20
10
5
1
-2.26
-0.87
0.51
1.90
3.29
Internally Studentized Residuals
Color points by value of
All effects
99.8
57.61

Fig.2

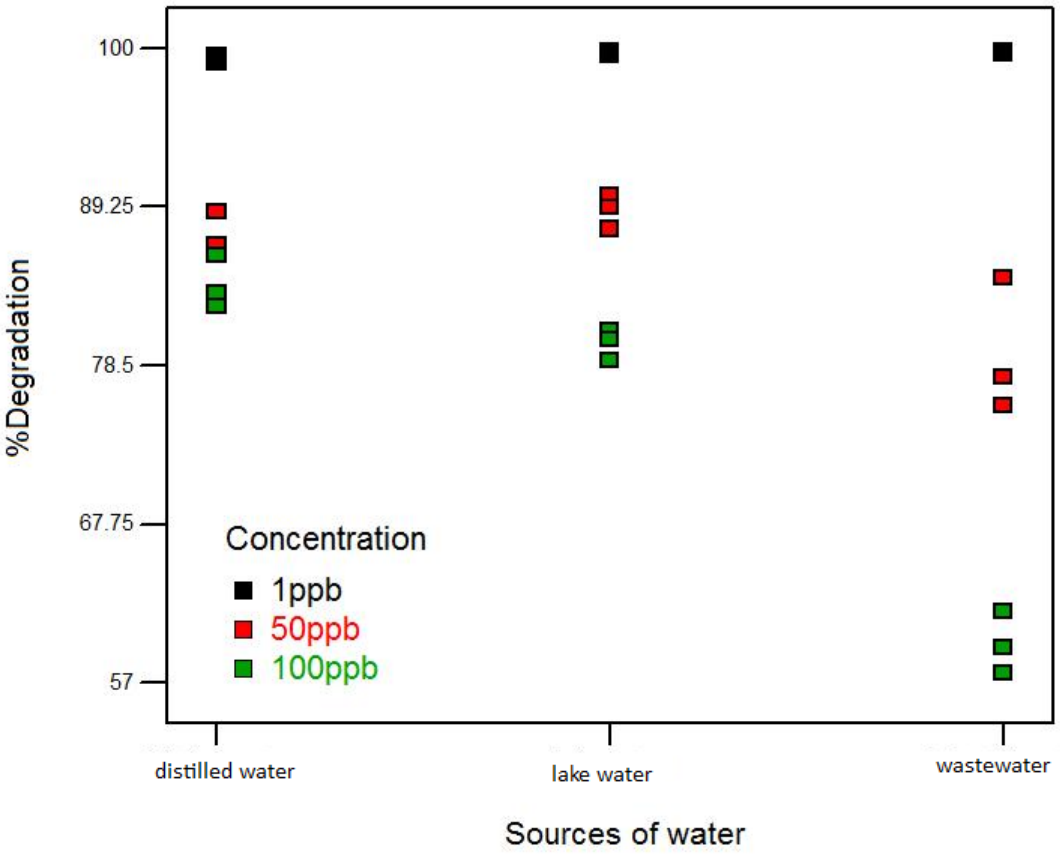
100
89.25
78.5
67.75
57
%Degradation
Concentration
1ppb
50ppb
100ppb
distilled water
lake water
wastewater
Sources of water

Fig. 3

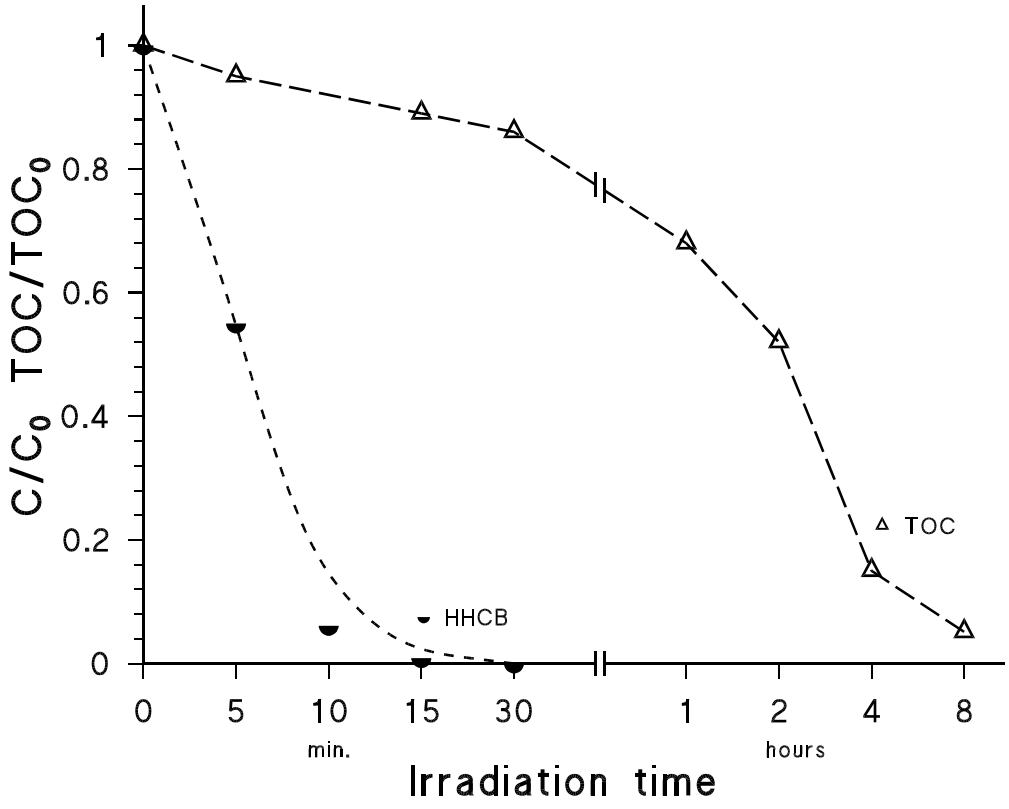
C/C0 TOC/TOC0
1
0.8
0.6
0.4
0.2
0
TOC
HHCB
0
5
10
15
30
1
2
4
8
min.
hours
Irradiation time

Fig. 4

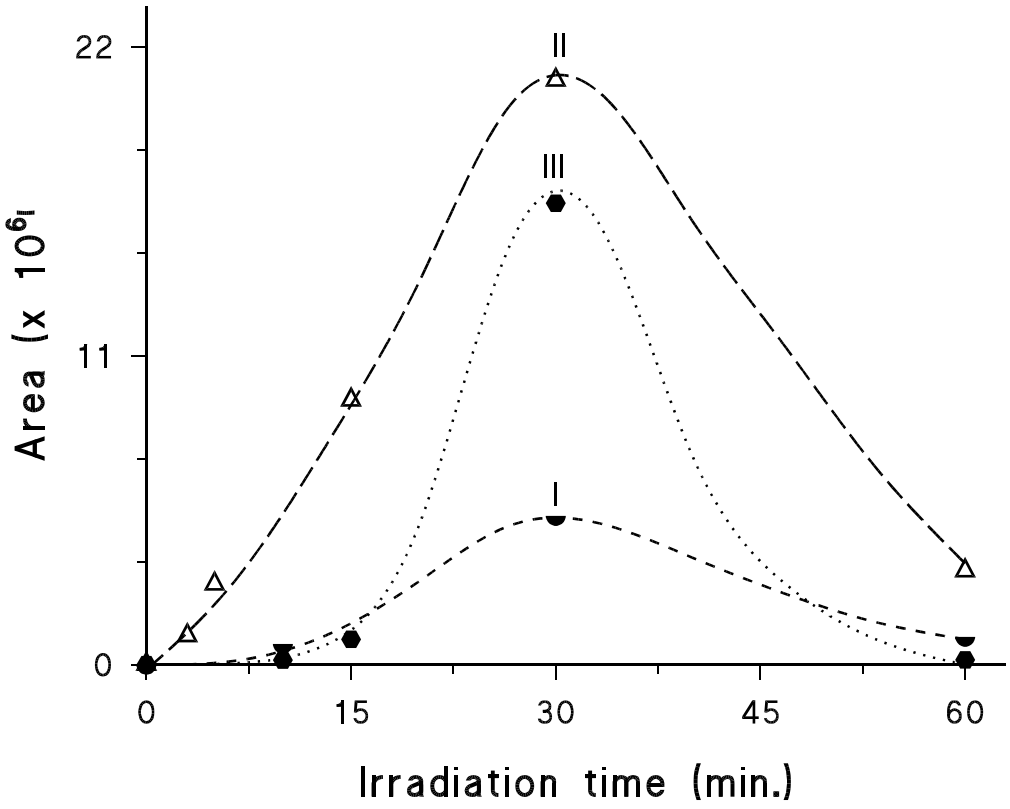

Fig. 5

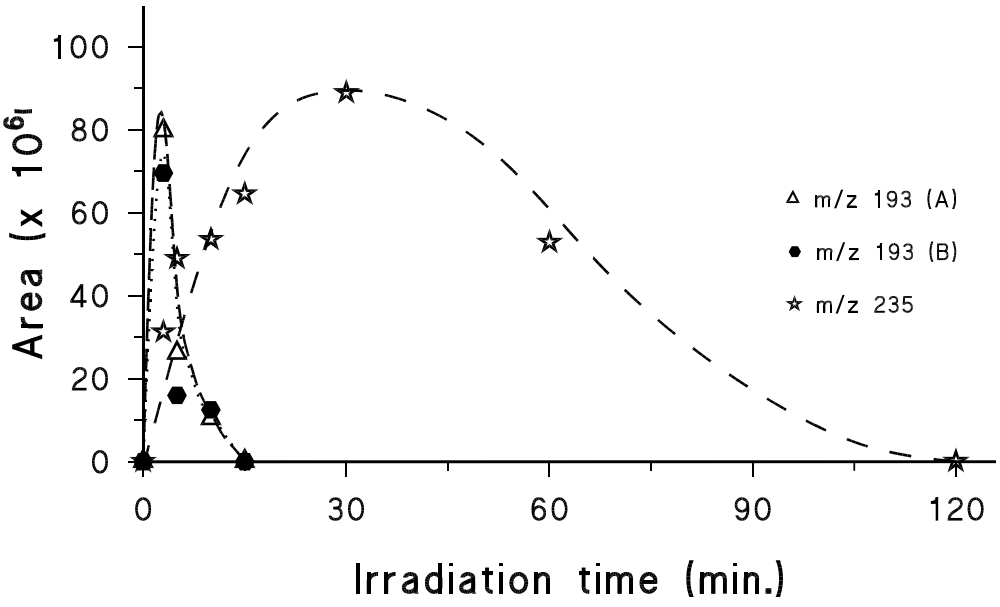
100
80
60
40
20
0
Area (x 10⁶I
0
30
60
90
120
Irradiation time (min.)
m/z 193 (A)
m/z 193 (B)
m/z 235

Fig. 6

Table 1. Design matrix and response data for photocatalytic degradation of HHBC

Std	Run	A: Sources of water	B: Concentration in ppb	% Degradation
2	1	Distilled water	1	99
18	2	Wastewater	50	84.38
15	3	Lake water	50	89.21
20	4	Distilled water	100	85.9
22	5	Lake water	100	78.83
26	6	Wastewater	100	61.8
5	7	Lake water	1	99.75
13	8	Lake water	50	87.71
17	9	Wastewater	50	75.74
10	10	Distilled water	50	86.19
16	11	Wastewater	50	77.66
3	12	Distilled water	1	99.5
9	13	Wastewater	1	99.8
14	14	Lake water	50	89.96
25	15	Wastewater	100	57.61
27	16	Wastewater	100	59.34
21	17	Distilled water	100	83.37
11	18	Distilled water	50	88.86
4	19	Lake water	1	99.58
23	20	Lake water	100	80.81
24	21	Lake water	100	80.23
8	22	Wastewater	1	99.7
6	23	Lake water	1	99.51
19	24	Distilled water	100	82.47

12	25	Distilled water	50	86.59
7	26	Wastewater	1	99.57
1	27	Distilled water	1	99.21

Table 2. ANOVA for selected nested factorial model

ANOVA for water matrix (Error term includes B, AB)						
Source	Sum of Squares	df	Mean Square	F Value	p-value Prob > F	Remarks
Model	638.77	2	319.39	0.57	0.5953	not significant
A-Sources of water	638.77	2	319.39	0.57	0.5953	not significant
Residual	3384.29	6	564.05			
Cor Total	4023.06	8				
ANOVA for HHCB initial concentration (Block term includes A)						
Block	638.77	2	319.39			
Model	3384.29	6	564.05	155.28	< 0.0001	significant
B-Concentration	2839.64	2	1419.82	390.87	< 0.0001	
AB	544.66	4	136.16	37.49	< 0.0001	
Pure Error	65.38	18	3.63			
Cor Total	4088.45	26				
ANOVA for all effects						
Model	4023.06	8	502.88	138.44	< 0.0001	significant
A-sources of water	*638.77*	*2*	*319.39*	*87.92*	< 0.0001	significant
B-Concentration	*2839.64*	*2*	*1419.82*	*390.87*	< 0.0001	significant
AB	*544.66*	*4*	*136.16*	*37.49*	< 0.0001	significant
Pure Error	65.38	18	3.63			
Cor Total	4088.45	26				

Table 3. Intermediate compounds formed from HHCB transformation and detected by GC/MS.

Compound	t_{RIT} (min.)	Ions (m/z)	Structure
HHCB	17.10	258 [30], 243 [100], 213 [36]	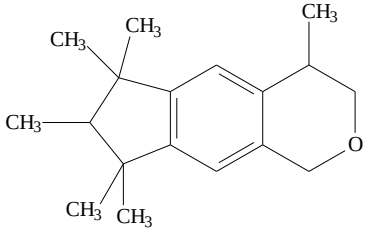
1,3,4,6,7,8-hexahydro-4,6,6,7,8,8-pentamethyl-oxo-cyclopenta[γ]-phenol (I)	12.81	218 [37], 203 [54], 175 [28], 161 [74], 150 [46], 135 [100], 107 [59], 152 [3]	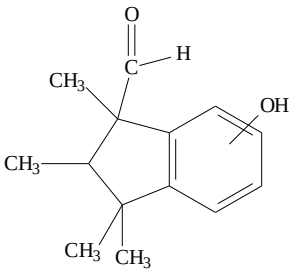
1,3,4,6,7,8-hexahydro-4,6,6,7,8,8-pentamethyl-oxo-cyclopenta[γ]-dihydroxybenzene (II)	16.08	234 [24], 219 [100], 185 [19], 73 [44], 57 [41]	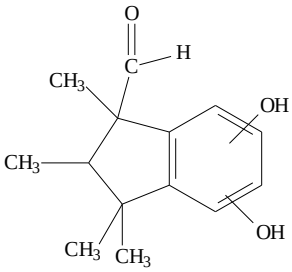
1,3,4,6,7,8-hexahydro-4,6,6,7,8,8-hexamethylcyclopenta[γ]-2-hydroxybenzopyran (III)	17.69	231 [100], 275 [35]	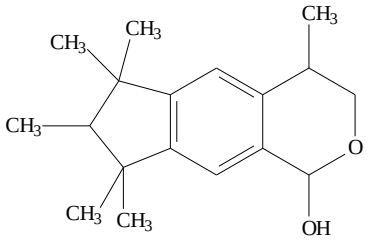

Table 4. Intermediate compounds formed from HHCB transformation and detected by HPLC/MS.

$[M+H]^+$	**t_{RIT} (min.)**	**Δ mmu**	**MS^2**	**Δ mmu**	**MS^3**	**Δ mmu**
193.0464 (A) $C_{10}H_9O_4$ **(IV)**	14.16	0.135	165.0153 $C_8H_5O_4$ ($-C_2H_4$) [100]	-2.975	137.0210 $C_7H_5O_3$ (-CO) [100]	-2.351
					121.0263 $C_7H_5O_2$ ($-CO_2$) [7]	-2.126
193.0464 (B) $C_{10}H_9O_4$ **(V)**	14.66	0.135	119.0467 C_8H_7O ($-C_2H_2O_3$) [100]	-2.491	91.0523 C_7H_7 (-CO) [100]	1.937
235.1809 $C_{15}H_{23}O_2$ **(VI)**	9.67	11.564	113.1303 C_8H_{17} ($-C_7H_6O_2$) [1]	-2.491	-	-
			86.0946 C_6H_{14} ($-C_9H_9O_2$) [100]	-14.442	-	-